Data Article

Dataset for electronic and optical properties of Y_2O_2S and Er dopped Y_2O_2S calculated using density functional theory and simulated x-ray near edge spectra

Nicholas Dimakis [a],[*], Eric Baldemar Rodriguez Jr [b],
Kofi Nketia Ackaah-Gyasi [c], Madhab Pokhrel [a]

[a] Department of Physics and Astronomy, University of Texas Rio Grande Valley, Edinburg 78539, USA
[b] Department of Mechanical Engineering, University of Texas Rio Grande Valley, Edinburg 78539, USA
[c] Department of Computer Science, University of Texas Rio Grande Valley, Edinburg 78539, USA

ARTICLE INFO

ABSTRACT

The computational data presented in this paper refer to the research article "Optical properties and simulated x-ray near edge spectra for Y_2O_2S and Er doped Y_2O_2S". We present the data used to calculate the structural, electronic, and optical properties of the Y_2O_2S and its Er^{+3} doped counterparts at various concentrations using density functional theory (DFT) and simulated X-ray near edge (XANES) spectra. We report electronic information from DFT and DFT+U generated from the Vienna Ab initio Simulation Package (VASP) using PAW pseudopotentials. We also report VASP calculated optical properties for the host Y_2O_2S using the independent particle approximation (IPA), the random phase approximation (RPA), the many-body GW_0 approximation, and the Bethe-Salpeter equation (BSE) approximation, under the 10-atom unit cell. The IPA calculations are repeated using the 80-atom unit cell for both the host Y_2O_2S and the $Y_2O_2S:Er^{+3}$ counterparts. The optical properties data include the frequency-dependent real and imaginary parts of the dielectric function, the absorption and extinction coefficients, the refractive index, and the reflectivity. FEFF10 XANES calculations are per-

formed on the Y K-, L_1-, L_2-, and L_3-edges, as well as on the Er M_5-edge.

Specifications Table

Subject	Physics, Chemistry
Specific subject area	Computational Chemistry, Material Science
Type of data	Table
	Figure
How the data were acquired	Optimized geometries, electronic structure, and optical properties were calculated using the VASP program. XANES data were calculated using the FEFF10 code.
Data format	Raw
	Analyzed
Description of data collection	All calculations were performed at the Texas Advanced Computing Center under the Lonestar 6 and Stampede 2 supercomputers using VASP and FEFF 10 codes.
Data source location	• Institution: University of Texas Rio Grande Valley
	• City/Town/Region: Edinburg, TX
	• Country: USA
Data accessibility	Repository name: Mendeley Data
	Data identification number (DOI number): 10.17632/bym3yj3xxc.1
	Direct link to the dataset: https://doi.org/10.17632/bym3yj3xxc.1
Related research article	N. Dimakis, E.B. Rodriguez. Jr., K.N. Ackaah-Gyasi, M. Pokhrel, Optical properties and simulated x-ray near edge spectra for Y_2O_2S and Er doped Y_2O_2S, Materials Today Communications, 33 (2022) 104328 [1]. https://doi.org/10.1016/j.mtcomm.2022.104328

Value of the Data

- We provide the data for the structural, electronic, and optical properties of Y_2O_2S and $Y_2O_2S:Er^{+3}$ at various Er concentrations using several computational approaches. These data are useful to experimentalists for predicting the Y_2O_2S bandgap and it's change due to Er doping.
- We provide calculated X-ray absorption near edge structure (XANES) spectra using the FEFF 10 code, which can be used by experimentalists to analyse transitions in the Y and Er X-ray edges. These data also include projected densities of states per orbital, which are used for electron transition assignments at the X-ray pre-edge and edge regions.
- We provide data from different approximations on calculating optical properties, thus showing their accuracy relative to experiments. These data can also be used by computational chemists for further improvement.

  Our electronic calculations show the presence of the partially filled Er-4f band at the Fermi energy, which agrees with the experimentally observed Er f-f intraband transitions.

1. Objective

This dataset can be used by computational material scientists to reproduce the electronic and optical properties calculations and explore how the parameters used in the input files affected the calculations' accuracies for $Y_2O_2S:Er^{+3}$ under varying Er concentrations. Moreover, the Vienna Ab initio Simulation Package (VASP) and FEFF 10 input files contain parameters that can be used for similar calculations of other materials. The data reported for optical properties

calculations for the host Y_2O_2S refer to different approximations, which affect accuracy, when compared with experimental data. The most accurate approaches for optical properties calculations (i.e., GW and BSE) are not always feasible due to the size of the supercell. In this case, our data show that optical properties calculations using the least accurate IPA method provide sufficiently accurate results relative to the more CPU and memory demanding RPA methods, for energies up to 25 eV. Overall, this dataset adds value to the original published article due to the reproducibility of the data.

2. Data Description

Fig. 1 shows the geometrically optimized unit cells used in our periodic density functional theory (DFT) [2] and FEFF 10 calculations, as well as the molecular clusters used in our FEFF 10 [3] calculations for the $Y_2O_2S:Er^{+3}$ under 3.125%, 6.25%, and 9.175% concentrations. The DFT calculations are performed using the 10-atom and 80-atom unit cell. The FEFF 10 calculations for the $Y_2O_2S:Er^{+3}$ require large clusters, where the absorbing atom is close to the center of the cluster. For the host Y_2O_2S, the FEFF calculations use a periodic k-space approach [4]. DFT and DFT+U [5] are used to calculate the Y_2O_2S and the $Y_2O_2S:Er^{+3}$ bandgaps, whereas the many-body GW_0 approximation is also used for the bandgap of the host $Y_2O_2S:Er^{+3}$ (Table 1). DFT underestimates the bandgaps relative to experiments, whereas DFT+U improves the bandgap value. However, this improvement is fortuitous, since DFT+U alters the conduction band and changes the bandgap from indirect to direct, in contrast with the experiments. The GW_0 overestimates the bandgap, whereas the best agreement is obtained from the BSE approximation.

Fig. 2 shows the frequency-dependent dielectric function using GW_0 [6, 7] under the independent particle method (IPA) [8, 9], the random phase approximation (RPA) [10], and the BSE [11] approximation. The BSE provides accurate bandgap and excitonic information. The BSE and
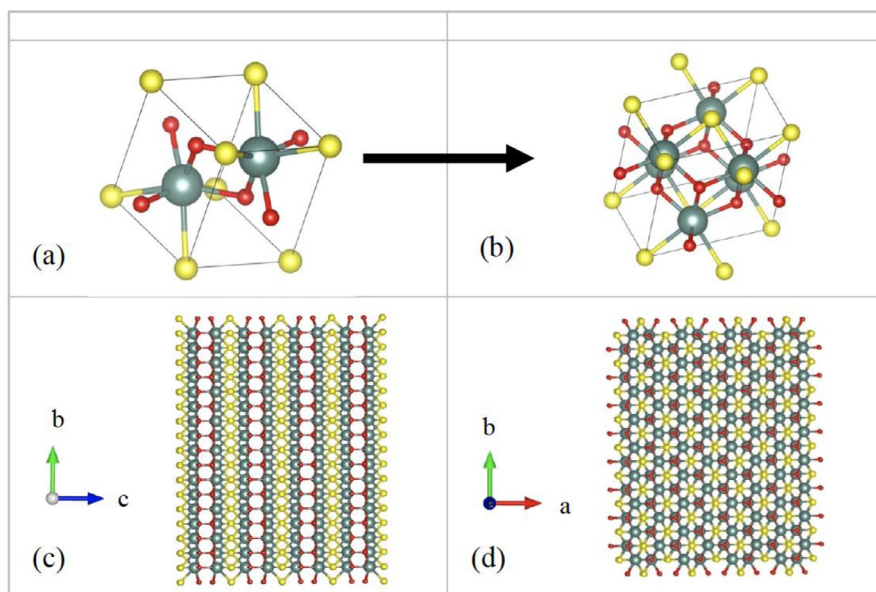

Fig. 1. (a) The Y_2O_2S unit cell in its triclinic form used for the k-space FEFF 10 calculations and (b) in a cubic form after using the transformation of eq. (1) for i = 1, used by DFT (b), and (c) FEFF 10 geometry configurations for $Y_2O_2S:Er^{+3}$, with the absorbing Er atom located close to the center of the cuboid. Thin lines denote the unit cell boundaries. Atoms are colors as follows: Y, O, and S are green, red, and yellow, respectively.

Table 1
Bandgaps (E_g) for the Y_2O_2S and its Er^{+3} doped counterparts per method used.

Y_2O_2S	Method			
	DFT	DFT+U	GW_0+IPA[b]	GW_0+BSE
	E_g (eV)			
Y_2O_2S	3.01	3.80[a]	5.30	5.08
Y_2O_2S: 3.125 % Er^{+3}	2.73, 0.13	2.92[a], 0.13[a]		
6.25 % Er^{+3}	2.75, 0.18	2.96[a], 0.34[a]		
9.175 % Er^{+3}	2.77, 0.20	2.94[a], 0.38[a]		

[a] DFT+U data with $U_d(Y) =12$ eV and $J_d(Y) = 1$ eV.
[b] Same as GW_0+RPA[b].
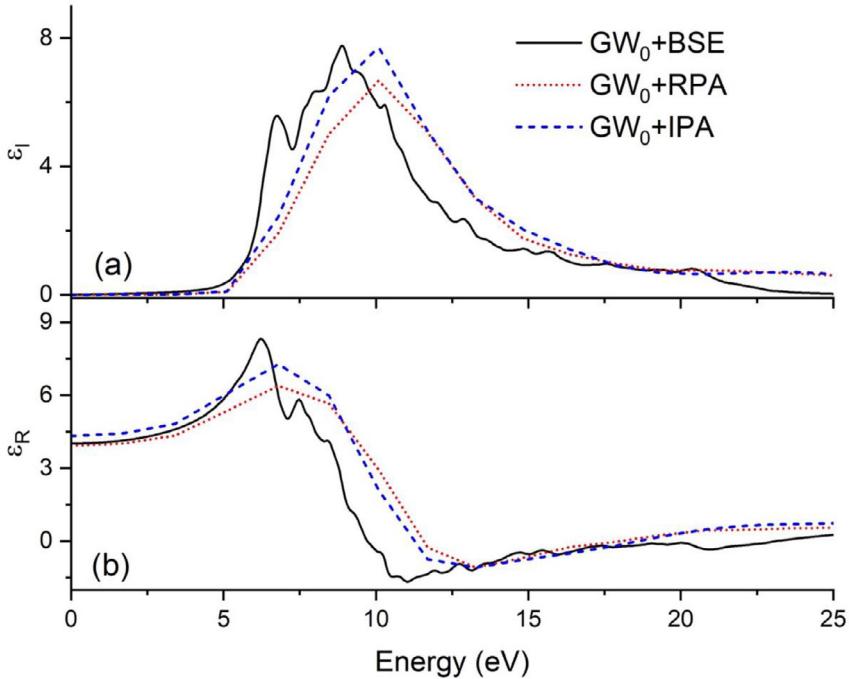
Fig. 2. (a) The imaginary part of the frequency-dependent dielectric function (ε_I) using GW_0 under the IPA, RPA, and BSE and (b) the real part (ε_R).

the GW_0 show similar values for the static dielectric constant $\varepsilon_R(0)$, whereas the best agreement with experiments is provided by the GW_0 under the IPA.

Fig. 3 shows the frequency-dependent extinction coefficient $\kappa(\omega)$ for the host Y_2O_2S and its Er^{+3} doped counterparts under the 80-atom cell. The GW_0 calculations show a shift on the $\kappa(\omega)$ onsite, in agreement with the larger bandgap predicted by GW_0 relative to DFT. The $\kappa(\omega)$ spectrum for the Y_2O_2S:Er^{+3} at the energies below the bandgap show several peaks, which correspond to the Er f-f intraband transitions.

Table 2 shows the static refractive index and reflectivity, as well as the maximum of the refractive index, the reflectivity, and the absorption coefficient, for the host Y_2O_2S and its Er doped counterparts. The energy locations for the above maximum values are also given. The denser $8 \times 8 \times 8$ Brillouin zone (BZ) grid does not significantly change the optical properties of the host Y_2O_2S. Increased Er doping increases the static refractive index and reflectivity. For the host Y_2O_2S, the static values of the refractive index and reflectivity are larger for the IPA and lower for the GW_0+RPA. Table 3 shows the FEFF calculated X-ray edges of Y and Er, which are com-
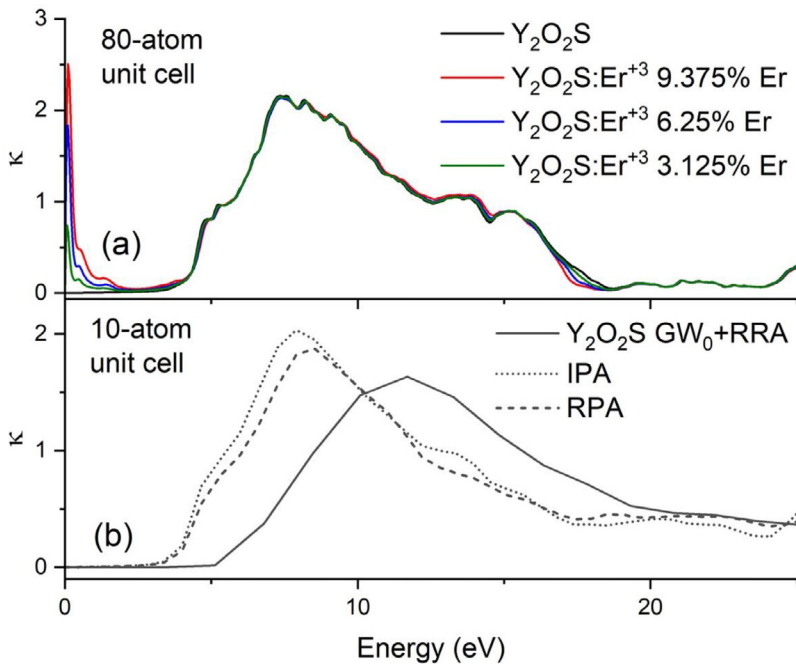
Fig 3. The frequency-dependent extinction coefficient $\kappa(\omega)$ for (a) the undoped Y_2O_2S and its Er^{+3} doped counterparts using the IPA and the 80-atom unit cell and (b) the undoped Y_2O_2S using the 10-atom unit cell under the IPA, RPA, and GW_0+RPA.

Table 2

The static refractive index n(0) and reflectivity R(0), the maximum values of the refractive index $n(\omega)_{max}$, reflectivity $R(\omega)_{max}$, and absorption coefficient $\alpha(\omega)_{max}$ and their locations in the energy spectra per method and unit cell configuration for the host Y_2O_2S and its doped counterparts. The energy locations ω are given in parentheses. Values in square brackets refer to the calculations using the Γ-centered $8 \times 8 \times 8$ grid, whereas all other values were obtained using the $6 \times 6 \times 6$ grid.

	Material & Method					
	Y_2O_2S			$Y_2O_2S{:}Er^{+3}$		
				3.125% Er	6.25% Er IPA[2]	9.375 % Er
Property	IPA	RPA	GW_0+RPA			
n(0)	2.31 [2.33] [1]	2.17 [2.19]	1.98			
	2.28[2]			3.43	5.17	6.16
$n(\omega)_{max}$	3.11 [3.06] [1]	2.86 [2.85]	2.58			
(ω)	4.68 [4.68] [1]		8.49			
$n(\omega)_{max}$	3.24[2]			3.21	3.19	3.17
(ω)	4.52[2]			4.54	4.59	4.64
R(0)	15.89 [16.03] [1]	13.96 [13.96]	10.87			
	15.42[2]			30.34	36.04	51.45
$R(\omega)_{max}$	41.17 [39.91]	38.78 [37.20]	34.19			
(ω)	8.5 [8.52]		13.28			
$R(\omega)_{max}$	45.84[2]			45.35	45.03	44.93
(ω)	9.57[2]			9.59	9.60	9.66
$\alpha(\omega)_{max}$	1.70 [1.68]	1.66 [1.62]	1.944			
(ω)	8.50 [8.52]		11.66			
$\alpha(\omega)_{max}$	1.80			1.74	1.69	1.75
(ω)	9.07			8.26	7.44	8.30

[1] 10 atom unit cell.
[2] 80 atom unit cell.

Table 3

X-ray Y and Er edges as calculated by FEFF 10 and compared with experimental data.

Element	X-ray edge	Experimental	FEFF
Y	K	17038.4	17059.95
	L_1	2372.5	2387.81
	L_2	2155.5	2157.40
	L_3	2080.0	2082.14
Er	L_3	8357.9	8354.04
	M_5	1409.0	1425.33

pared with experimental data. A good agreement between the calculated and the experimentally reported values is obtained for the Y L_2- and L_3- edges and the Er L_3-edge.

The submitted data are grouped in four directories. Three of these four directories contain data which refer to the doped $Y_2O_2S:Er^{+3}$ compounds at 3.125%, 6.25%, and 9.175% and Er concentrations and are named "Y_2O_2S-xEr", where x is 3, 6, and 9. The fourth directory contains data related to the host Y_2O_2S. Each of the Y_2O_2S-xEr directories contain three subdirectories, where files from FEFF, band structure, and optical properties calculations reside. Moreover, each of the last two directories contain DFT and DFT+U VASP input files and data files that were used for plotting Fig. 3a. The host Y_2O_2S contains three subdirectories, two that contain DFT VASP input files and data files used to plot Fig. 2 and Fig 3b. These subdirectories are named using the number of atoms in unit cell (i.e., 10- and 80-atom). The last subdirectory contains the host Y_2O_2S FEFF files.

3. Computational Design, Materials and Methods

3.1. Unit cell modeling

The Y_2O_2S unit cell in a triclinic form (space group $P\bar{3}m1$) is used to build 10- and 80-atom supercells in cubic form for Y_2O_2S doped with Er^{+3} by using the following transformation matrix

$$T = x \cdot \begin{pmatrix} 1 & 1 & 0 \\ -1 & 1 & 0 \\ 0 & 0 & 1 \end{pmatrix}\Big|_{x=1,2} \tag{1}$$

The unit cell has 5 unique atoms as follows: 2 Y, 2 O, and 1 S atom. The XANES spectra for the Y_2O_2S: Er^{+3} cases are calculated using 140 atoms clusters of radii $\sim$ 7.9 Å around the absorbing Er atom.

3.2. DFT parameters

We use the periodic DFT code VASP [12–15] to calculate electronic and optical properties of Y_2O_2S and Y_2O_2S doped with Er^{+3} at 3.175 %, 6.25 %, and 9.375 % Er^{+3} concentrations. The VASP PAW pseudopotentials were used [16, 17] with Y, O, S, and Er valance electron configurations as $4s^2 4p^6 5s^1 4d^2$, $2s^2 2p^4$, $3s^2 3p^4$, and $5s^2 5p^6 4f^{11} 5d^1 6s^2$, respectively. The generalized gradient approximation of the Perdew–Burke–Ernzerhof (PBE) functional [18] was used. The long-range electron correlations responsible for van der Waals interactions were approximated by the Grimme [19] D3 semiempirical correction. We used 525 eV for the kinetic energy cutoff for all our calculations, which exceeds the maximum of the default PAW energy cutoff values. The energy SCF convergence and the geometry thresholds are set to 10^{-9} eV per atom and 10^{-4} eV/Å, respectively. The BZ was sampled using the 4 × 4 × 4 Monkhorst-Pack grid for geometry optimizations and electronic information, whereas for the optical properties we used the Γ-centered

$6 \times 6 \times 6$ BZ grid. The electronic band structure and the densities of states (DOS) are calculated using two district methods: 1) DFT and 2) DFT+U, where U is the Hubbard U correction parameter by Liechtenstein et. al [5]. The optical properties for the host Y_2O_2S are calculated using the IPA, the RPA, the many-body GW_0 methods as a correction to IPA and RPA (i.e., GW_0+IPA and GW_0+RPA), and the BSE approximation [11], the last four using the 10-atom unit cell. The $Y_2O_2S:Er^{+3}$ optical properties were calculated using the IPA method, under the 80-atom unit cell.

3.3. FEFF 10 parameters

The FEFF10 code [3] is used to calculate XANES through real space Green functions. The atomic potentials have been calculated self-consistently. We include full multiple scattering in all FEFF 10 calculations. The Hedin-Lundqvist pseudopotential [20] was used for the exchange interaction, whereas the absorbing atom core hole was treated using the RPA method. FEFF also calculates projected DOS per atomic orbital. We used 0.1 eV half-width as the Lorentzian parameter for the projected DOS calculations.

Ethics Statements

This work does not require any ethical statement.

CRediT Author Statement

Nicholas Dimakis: Conceptualization, Methodology, Supervision, Validation, Writing – reviewi & editing; **Eric Baldemar Rodriguez Jr.:** Data curation, Validation, Investigation; **Kofi Nketia Ackaah-Gyasi:** Data curation, Validation, Investigation; **Madhab Pokhrel:** Conceptualization, Methodology, Writing – review & editing, Data curation, Validation.

Declaration of Competing Interest

The authors declare that they have no known competing financial interests or personal relationships that could have appeared to influence the work reported in this paper.

Acknowledgments

References

[1] N. Dimakis, E.B. Rodriguez Jr., K.N. Ackaah-Gyasi, M. Pokhrel, Optical properties and simulated x-ray near edge spectra for Y_2O_2S and Er doped Y_2O_2S, Mater. Today Commun. 33 (2022) 104328.

[2] W. Kohn, L.J. Sham, Self-consistent equations including exchange and correlation effects, Phys. Rev. 140 (1965) A1133–A1138.

[3] J.J. Kas, F.D. Vila, C.D. Pemmaraju, T.S. Tan, J.J. Rehr, Advanced calculations of X-ray spectroscopies with FEFF10 and Corvus, J. Synchrotron Rad. 28 (2021) 1801–1810.

[4] K. Jorissen, J.J. Rehr, Calculations of electron energy loss and x-ray absorption spectra in periodic systems without a supercell, Phys. Rev. B 81 (2010) 245124.

[5] A.I. Liechtenstein, V.I. Anisimov, J. Zaanen, Density-functional theory and strong interactions: orbital ordering in Mott-Hubbard insulators, Phys. Rev. B 52 (1995) R5467–R5470.

[6] F. Aryasetiawan, O. Gunnarsson, The GW method, Rep. Prog. Phys. 61 (1998) 237–312.

[7] W.G. Aulbur, L. Jönsson, J.W. Wilkins, Quasiparticle calculations in solids, J. Phys. C Solid State Phys. 54 (2000) 1–218.

[8] S.L. Adler, Quantum theory of the dielectric constant in real solids, Phys. Rev. 126 (1962) 413–420.

[9] N. Wiser, Dielectric constant with local field effects included, Phys. Rev. 129 (1963) 62–69.

[10] H. Ehrenreich, M.H. Cohen, Self-consistent field approach to the many-electron problem, Phys. Rev. 115 (1959) 786–790.

[11] E.E. Salpeter, H.A. Bethe, A relativistic equation for bound-state problems, Phys. Rev. 84 (1951) 1232–1242.

[12] G. Kresse, J. Hafner, Ab initio molecular dynamics for liquid metals, Phys. Rev. B 47 (1993) 558(R)-561(R).

[13] G. Kresse, J. Hafner, Ab initio molecular-dynamics simulation of the liquid-metal–amorphous-semiconductor transition in germanium, Phys. Rev. B 49 (1994) 14251–14269.

[14] G. Kresse, J. Furthmüller, Efficiency of ab-initio total energy calculations for metals and semiconductors using a plane-wave basis set, Comput. Mater. Sci. 6 (1996) 15–50.

[15] G. Kresse, J. Furthmüller, Efficient iterative schemes for ab initio total-energy calculations using a plane-wave basis set, Phys. Rev. B 54 (1996) 11169–11186.

[16] P.E. Blöchl, Projector augmented-wave method, Phys. Rev. B 50 (1994) 17953–17979.

[17] G. Kresse, D. Joubert, From ultrasoft pseudopotentials to the projector augmented-wave method, Phys. Rev. B 59 (1999) 1758–1775.

[18] J.P. Perdew, K. Burke, M. Ernzerhof, Generalized gradient approximation made simple, Phys. Rev. Lett. 77 (1996) 3865–3868.

[19] S. Grimme, J. Antony, S. Ehrlich, H. Krieg, A consistent and accurate ab initio parametrization of density functional dispersion correction (DFT-D) for the 94 elements H-Pu, J. Chem. Phys. 132 (2010) 154104–154118.

[20] L. Hedin, B.I. Lundqvist, Explicit local exchange-correlation potentials, J. Phys. C Solid State Phys. 4 (1971) 2064–2083.